Published by Institute of Physics Publishing for SISSA

Received: *February 20, 2007*
Revised: *March 27,2007*
Accepted: *April 13, 2007*
Published: *April 20, 2007*

Geometric scaling and QCD dynamics in DIS

Emil Avsar and Gösta Gustafson

Dept. of Theoretical Physics,
Sölvegatan 14A, S-223 62 Lund, Sweden
E-mail: Emil.Avsar@thep.lu.se, Gosta.Gustafson@thep.lu.se

Abstract: DIS data from HERA show a striking regularity as $\sigma^{\gamma^* p}$ is a function of the ratio $\tau = Q^2/Q_s^2(x)$ only. The scaling function shows a break at $\tau \approx 1$, which has been taken as an indication for saturation. However, besides saturation also the transition between dominance of $k_\perp$-ordered (DGLAP) and $k_\perp$-non-ordered (BFKL) evolution contributes to a break around this value of τ, as well as the suppression for small Q^2 due to finite quark masses and confinement. In this paper we use a dipole cascade model based on Mueller's dipole model, which also includes energy conservation and pomeron mergings, to investigate the contributions of these different effects to the scaling behaviour. As a result we predict that the scaling function for $\tau < 1$ will be modified when data for $Q^2 > 1\,\mathrm{GeV}^2$ become available. We also investigate the scaling properties of the charm contribution and the impact parameter dependence of the saturation scale.

Keywords: Phenomenological Models, Deep Inelastic Scattering, QCD.

JHEP04(2007)067

Contents

JHEP04(2007)067

1. Introduction

Data from deep inelastic scattering (DIS) experiments at small-x exhibits an interesting property called geometric scaling [1]. This means that the total $\gamma^* p$ cross section is not a function of the two variables x and Q^2 separately but rather a function of the combination $Q^2/Q_s^2(x)$ only, where the "saturation scale" Q_s is defined such that saturation is expected to occur at Q-values below Q_s.

DIS is quite successfully described by the Golec-Biernat-Wüsthoff (GBW) model [2, 3] in which the virtual photon splits into a $q\bar{q}$ dipole long before the interaction with the proton. The GBW model is also called the saturation model, since it explicitely assumes that the dipole-proton cross section, σ_{dp}, saturates to a constant value σ_0 as the dipole size, r, gets large. To be more precise, the GBW model assumes that

$$\sigma_{\mathrm{dp}} = \sigma_0\{1 - \exp(-r^2/4R_0^2(x))\}, \tag{1.1}$$

where the "saturation radius" $R_0(x)$, identified with $Q_s^{-1}(x)$, decreases with decreasing x. In the GBW fit Q_s^2 has the form

$$R_0^{-2} = Q_{s,GW}^2 = Q_0^2 \left(\frac{x_0}{x}\right)^\lambda \quad \text{with } Q_0 = 1\text{GeV}, \, x_0 = 3{\cdot}10^{-4}, \, \lambda = 0.29. \tag{1.2}$$

We thus see that $\sigma_{\rm dp}$ is a function of $r/R_0(x)$ only, and consequently it satisfies "geometric scaling". For massless quarks this also implies that the $\gamma^* p$ cross section is a scaling function of $\tau = Q^2 R_0^2 = Q^2/Q_{s,GW}^2$, and this feature is indeed confirmed by experimental data as demonstrated in ref. [1]. (This reference also finds scaling if the relation $\ln R_0^2 \sim \lambda \ln x$ is replaced by $\ln R_0^2 \sim -x^{-0.08}$.)

Plotting the observed $\gamma^* p$ cross section as a function of τ one can also see that the growth of the cross section towards smaller τ is reduced noticeably when $\tau \lesssim 1$, corresponding to values satisfying $Q^2 \lesssim Q_{s,GW}^2$. Later analyses including DGLAP evolution for larger Q^2 [4] improve the agreement with the HERA data, with the consequence that saturation is beginning at somewhat smaller τ-values. This good agreement together with the success of the GBW model in describing diffractive data, has been taken by some authors as a proof that saturation exists, and that it has been observed at HERA.

Including the finite quark mass in the wavefunction describing the $\gamma^* - q\bar{q}$ coupling introduces scale-breaking effects. In particular the charm quark gives a large contribution to the cross section, which is phased out for $Q^2 \lesssim 4m_c^2$. In ref. [2] a fit including the charm quark mass actually shifts the expected onset of saturation to much smaller x-values, with $x_0 = 0.4{\cdot}10^{-4}$ in the expression for R_0 or Q_s in eq. (1.2). Such a shift is confirmed in the analysis in ref. [5], which includes the mass of the charm and beauty quarks into the DGLAP-improved formalism of ref. [4].

For small Q^2 also the mass of the light quarks becomes important. In refs. [1, 2] this is taken into account by replacing the variable $x = Q^2/W^2$ in the definition of R_0 or $Q_{s,GW}$ by

$$\bar{x} = x(1 + 4m_f^2/Q^2) = \frac{Q^2 + 4m_f^2}{W^2}. \tag{1.3}$$

In this way the scaling relation can be studied also for very small Q^2 and for photoproduction.

The test of scaling in the region of small τ is, however, limited by the fact that small values of τ are reached *only* for small Q^2, since larger Q^2-values would need energies not accessible at the HERA accelerator. Thus the data for $\tau < 0.5 - 1$, where the change in the slope of the $\gamma^* p$ cross section is observed, are all obtained for Q^2-values smaller than $1\,\text{GeV}^2$, which means that they are all in the non-perturbative region. The limited kinematical range at HERA also implies that there is little overlap between data at different Q^2 for fixed τ, which implies that it is relatively easy to achieve a scaling result by adjusting the quark masses.

The question of scaling for $Q^2 > Q_s^2$ is discussed by Iancu et al. in ref. [6]. These authors argue that if Q_s^2 is defined as the scale where the scattering probability is of order 1, then the BFKL evolution equation implies that the quark and gluon distributions have to obey geometric scaling in the range $1 \lesssim \ln(Q^2/Q_s^2) \ll \ln(Q_s^2/\Lambda_{QCD}^2)$. This rather wide

range in Q^2 results from the fast diffusion in $\ln k_\perp^2$ and the fast growth towards small x in the leading log BFKL evolution. Beyond this range in Q^2 the BFKL diffusion is gradually replaced by the (not explicitely scaling) double leading log result.

A numerical analysis of the diffusion in the BK equation is presented by Golec-Biernat et al. [7], including non-leading effects from a running coupling and from the so called kinematical constraint. The result from a running α_s is that $\ln Q_s^2$ for high energies grows $\sim \sqrt{Y}$, rather than proportional to Y, as assumed in eq. (1.2). It also significantly reduces the diffusion into the region of large $k_\perp^2$. The kinematical constraint reduces this diffusion further, and these results therefore put a question mark for the large scaling region dominated by BFKL dynamics obtained in ref. [6]. A related work is presented by Kwieciński and Staśto [8], where they study DGLAP evolution starting from scaling initial conditions on the line $Q^2 = Q_s^2$, with Q_s^2 determined by some unspecified dynamics. The result from this approach is also that scaling is approximately preserved in a large domain above the line $Q^2 = Q_s^2$.

In the past few years it has been observed that a scaling feature is inherent in the asymptotic solutions to the evolution equations in high energy QCD. It was also realized that the non-linear Balitsky-Kovchegov (BK) equation, which is the mean field version of the more general Balitsky-JIMWLK hierarchy (B-JIMWLK), is similar to a certain type of equation, well known in statistical physics, called the Fisher-Kolmogorov-Petrovsky-Piscounov (FKPP) equation, which is known to have traveling wave solutions [9, 10]. Written for a function $u(x,t)$, which depends on x and the time t, the solution for large t has the form of a traveling wave, $u(x - vt)$, where v is the speed of the wave. The similarity is expressed by the fact that the BK equation lies in the same universality class as the FKPP equation.

More recently, the importance of fluctuations in small-x evolution has been better understood [11], and this has led to the modification of the original version of the B-JIMWLK hierarchy into a new hierarchy of equations, which include both fluctuations and saturation effects. These new equations are also referred to as pomeron loop equations, since they contain both pomeron splittings and pomeron mergings in the evolution. This hierarchy of equations can also be written as a single Langevin equation, which is very similar to what is called the stochastic-FKPP (s-FKPP) equation [11]. The study of the asymptotic behaviour of the solution to this equation leads to the prediction of a new type of scaling law, called diffusive scaling [12], which is expected to hold at very high energies. It ought to be emphasized that the traveling wave solutions discussed here are asymptotic solutions expected to be relevant at extremely high energies, and therefore cannot be used to explain the scaling observed in the HERA energy regime.

The above discussion raises three important questions:

- What is the importance of saturation for the scaling behaviour?
- What is the dynamical mechanism behind the scaling observed for $\tau > 1$, i.e. for $Q^2 > Q_s^2$?
- Will the cross section still be scaling for $\tau \lesssim 1$, when data for larger Q^2 are available?

JHEP04(2007)067

In this paper we will argue that geometric scaling is expected also in the absence of saturation, and not only in the region dominated by BFKL diffusion, but also in the double leading log domain, where $k_\perp$-ordered (DGLAP) evolution chains are most important. Scaling appears naturally in a dipole cascade model [13, 14], which is based on Mueller's dipole evolution [15 – 17] but also includes energy-momentum conservation, pomeron merging, and a simple model for the proton. The MC implementation of the model reproduces both F_2 data from HERA and the total cross section in proton-proton scattering. This model shows geometric scaling for Q^2 below as well as above $Q^2_{s,GW}$, and for the one pomeron contribution as well as for the full unitarized result. In the model the transition between BFKL diffusion and $k_\perp$-ordered evolution occurs for Q^2 quite close to $Q^2_{s,GW}$, and there are three different effects which all contribute to the change in the scaling curve for $\tau \approx 0.5-1$: Saturation, the BFKL-DGLAP transition, and the finite effective masses for the light u-, d-, and s-quarks.

In order to get an intuitive understanding of the scaling feature we will besides the results of the MC simulations also discuss two simple approximations, which contain the basic features of DGLAP-BFKL evolution and the colour dipole cascades.

Diffractive excitation or rapidity gap events correspond to a large fraction of the events at HERA. Diffractive scattering is related to the impact parameter dependence of the interaction, and in section 8 we will discuss how the speed of the traveling wave varies with impact parameter, averaging out to the velocity observed in the experimental data.

The paper is organized as follows. In the next two sections we briefly discuss the DIS cross section, the concept of geometric scaling, and the dipole cascade approach to DIS. In section 4 we discuss the effect of the charm contribution together with the effect of saturation on the total cross section. In section 5, we present the two simple approximations to the full model as mentioned above. The scaling properties of the charm structure function are studied in section 6, and in section 7 we concentrate on the region $Q^2 < Q_s^2$ and study the effects of confinement and finite quark masses for small Q^2 below $1\,\mathrm{GeV}^2$ and the scaling properties of the cross section in this region. In section 8 we investigate the behaviour of the scattering amplitude for different impact parameters and how the scaling feature varies with impact parameter. Finally, in section 9, we reach at our conclusions.

2. DIS and geometric scaling

In the dipole description of DIS the virtual photon, long before the interaction with the proton, splits into a $q\bar{q}$ pair which then interacts with the proton. The transverse separation between the quark and the antiquark in such a dipole is denoted $\boldsymbol{r}$, and their fractions of the γ^* longitudinal momentum z and $1-z$. The coupling of the γ^* to the $q\bar{q}$ pair is well known and the leading order result reads

$$
\begin{aligned}
|\psi_L(z,r)|^2 &= \frac{6\alpha_{em}}{\pi^2}\sum_f e_f^2 Q^2 z^2(1-z)^2 K_0^2\left(\sqrt{z(1-z)Q^2+m_f^2}\,r\right)\\
|\psi_T(z,r)|^2 &= \frac{3\alpha_{em}}{2\pi^2}\sum_f e_f^2\left\{[z^2+(1-z)^2](z(1-z)Q^2+m_f^2)K_1^2\left(\sqrt{z(1-z)Q^2+m_f^2}\,r\right)\right.\\
&\quad \left. +m_f^2\,K_0^2\left(\sqrt{z(1-z)Q^2+m_f^2}\,r\right)\right\}. \qquad (2.1)
\end{aligned}
$$

Here ψ_L and ψ_T denote the longitudinal and transverse wave functions respectively. K_0 and K_1 are modified Bessel functions and the sum $\sum_f$ runs over all active quarks flavours, with mass m_f and electric charge e_f. The $\gamma^* p$ total cross section can then be written as

$$\sigma^{tot}_{\gamma^* p} = \int d^2\boldsymbol{r} \int_0^1 dz \{|\psi_L(z,r)|^2 + |\psi_T(z,r)|^2\} \sigma_{dp}(z,\boldsymbol{r}). \tag{2.2}$$

This cross section is related to the F_2 structure function via the relation

$$F_2 = \frac{Q^2}{4\pi^2 \alpha_{em}} \sigma^{tot}_{\gamma^* p}. \tag{2.3}$$

The factor $\sigma_{dp}(z,\boldsymbol{r})$ in (2.2) above denotes the dipole-proton cross section. In the GBW model this cross section is assumed to have the form given in eq. (1.1). If we only consider the three light quarks and neglect their masses, we see that the dipole size can be rescaled $r \to r/R_0$, which implies that the result only depends on the scaling variable $\tau \equiv Q^2/Q_s^2$.

The charm quark is known to give a significant contribution to the cross section, and the heavy charm quark must obviously have a large effect on the scaling properties. This will be discussed further in sections 4 and 6. However, also for the light quarks the finite masses will have significant effects for small Q^2, which will be discussed in section 7.

3. The dipole cascade model for DIS

We will in this section shortly describe the model we use to study the effect on geometric scaling from different features in the QCD evolution.

DIS at small x is dominated by gluonic cascades due to the $1/z$ singularity in the gluon splitting function. At large Q^2 the cascade can be described by DGLAP evolution, where the gluons are strictly ordered in transverse momentum. For smaller Q^2 also non-ordered gluon chains are important, and the $k_\perp$-ordered DGLAP evolution is replaced by the x-ordered BFKL evolution. The ordering in $k_\perp$ when $Q^2 \to \infty$ and the ordering in energy when $x \to 0$ follow both from an ordering in angle or, equivalently, in rapidity. Such an ordering is a consequence of soft gluon interference, and is the basis for the CCFM model [18, 19], which reproduces DGLAP and BFKL evolution in their respective domains of applicability with a smooth transition in between. The CCFM model is reformulated and generalized in the Linked Dipole Chain (LDC) [20] model. Here some emissions, which are treated as initial state radiation in CCFM, are instead included as final state radiation, with the result that the "non-Sudakov" formfactors disappear, and the cascade becomes symmetric when exchanging the role of the projectile and the target. The remaining gluons (called primary gluons in ref. [20] and backbone gluons in ref. [21]) define totally the structure of the final state.

At very high energies the density of gluons becomes very large, and nonlinear effects are needed to tame the exponential growth in the above linear evolutions, which would otherwise break the unitarity limit. Saturation and multiple interactions are easier to take into account in a formulation in transverse coordinate space since at high energies the transverse coordinate does not change between repeated subcollisions, while these collisions

do change the transverse momenta. This is exploited in the GBW dipole model and the dipole cascade model by Mueller [15 – 17].

The evolution in Mueller's model reproduces the leading order (linear) BFKL evolution. It starts from a colour singlet $q\bar{q}$ pair. The quark and the antiquark emit gluons coherently, forming a colour dipole. The original dipole is then split in two dipoles formed by the qg and $g\bar{q}$ systems. The new dipoles split repeatedly forming a dipole cascade. In the leading log approximation the probability per unit rapidity Y for a dipole with transverse coordinates $\boldsymbol{x}$ and $\boldsymbol{y}$ to split emitting a gluon at $\boldsymbol{z}$ is given by (to leading log accuracy $Y \equiv \ln 1/x$ and the true rapidity are equivalent)

$$\frac{d\mathcal{P}}{dY} = \frac{\bar{\alpha}}{2\pi} d^2\boldsymbol{z} \frac{(\boldsymbol{x}-\boldsymbol{y})^2}{(\boldsymbol{x}-\boldsymbol{z})^2(\boldsymbol{z}-\boldsymbol{y})^2} \tag{3.1}$$

The splitting probability in eq. (3.1) is singular for small dipole sizes $\boldsymbol{x}-\boldsymbol{z}$ or $\boldsymbol{z}-\boldsymbol{y}$. These singularities have to be screened by a cutoff, but the small dipoles have also a small probability to interact with the target, and therefore the total cross section is finite when the cutoff goes to zero. This implies that a lot of non-interacting virtual dipoles are created in the process, which also makes computer simulations difficult [22, 23].

It is well known that a significant part of next to leading corrections are related to energy-momentum conservation [24], and in refs. [25, 26] it is demonstrated that energy conservation has a large effect on the small x evolution. Relating the dipole size r to $1/k_\perp$ there are great similarities between Mueller's model and the LDC model. In ref. [13] these similarities were used to implement energy conservation in the dipole cascade formalism. The result is a dynamical cutoff for small dipoles, and the remaining emissions are ordered in both light cone variables p_+ and p_-, similar to the ordering in the LDC model. A dominant fraction of the virtual emissions is here eliminated, leaving mainly the "primary gluons" mentioned above. As a result the exponential growth for small x is significantly reduced. It also greatly improves the efficiency of the MC simulation, removing the difficulties encountered in refs. [22, 23].

Mueller's cascade includes saturation effects from multiple collisions in the Lorentz frame chosen for the calculation, but not the effects of pomeron merging in the cascades. The result is therefore not Lorentz frame independent. In ref. [14] we improved our model by allowing (colour suppressed) recouplings of the dipole chain during the evolution, a "dipole swing", which leads to an almost frame independent formalism. In this paper we also introduced a simple model for the proton in terms of three dipoles.

The dipole splitting is calculated in perturbative QCD, and therefore the model is meant to work in the perturbative regime, which means not too small Q^2. In figure 1 we show results for $\sigma^{\gamma^* p}$ as a function of the scaling variable $\tau \equiv Q^2/Q_s^2$ for different Q^2 above $0.3\,\mathrm{GeV}^2$. The results include both the dipole swing and multiple collisions and for $Q_s(x)$ we here use the definition by Golec-Biernat and Wüsthoff, given by (1.2). For these Q^2-values a scale-breaking effect is obtained from the charm mass, for which we use the value 1.4 GeV. The theoretical result is presented for the same kinematical variables as the experimental data, and we see that there is a very good agreement between theory and

JHEP04(2007)067

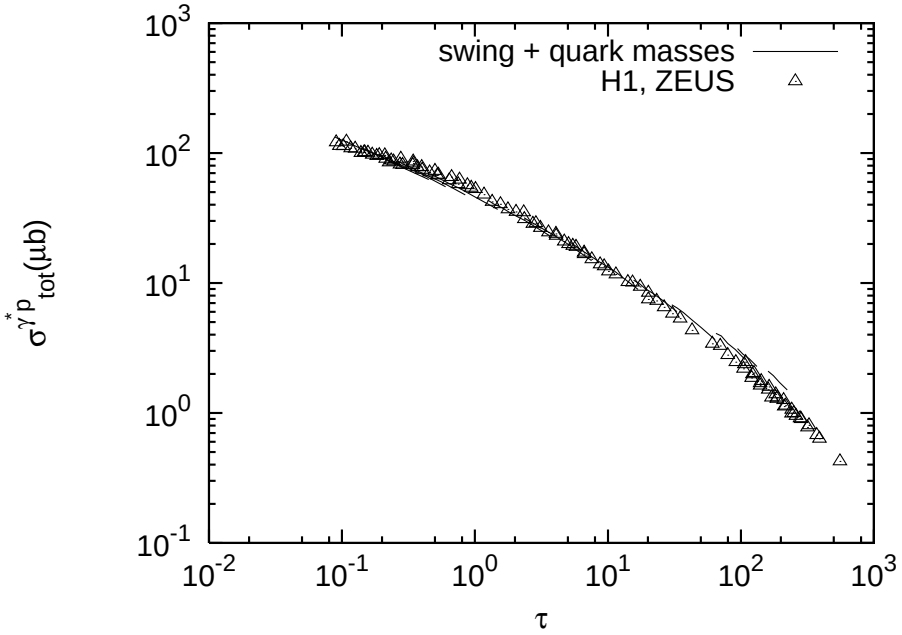

Figure 1: Our full results for the $\gamma^* p$ total cross section plotted as a function of the scaling variable $\tau = Q^2/Q^2_{s,GW}$. Here saturation effects are included both in the collision between the γ^* and the proton cascades and within the evolution in each individual cascade, via the so called dipole swing. We have used a charm mass of 1.4 GeV and an effective light quark mass of 60 MeV for the u, d and s quarks. Data points are taken from [27] and [28]. Results are presented for Q^2 ranging from 0.3 GeV^2 to 90 GeV^2, and with the same kinematics for the data and the model.

data. For small Q^2 the result is sensitive to confinement effects and effective quark masses. These problems will be further discussed in section 7.

4. Effects of saturation and the charm contribution

The effects of saturation and of the large charm quark mass are illustrated in figure 2. The results correspond to Q^2 between 0.75 and 90 GeV^2, and therefore the light quark masses can be neglected. The dotted lines show the results of the full model, presented in figure 1. The solid lines show the result when the charm mass is set to zero. The deviation between these curves therefore shows the effect of the charm quark mass. Neglecting also the swing gives the long-dashed curves, and finally including only the single pomeron term in the collisions gives the short-dashed curves. The difference between these and the solid lines therefore represents the effect of saturation.

We first note that saturation effects from multiple collisions and the swing have a relatively small effect for $\tau > 1$, but grow for smaller τ, and reduce the cross section by approximately a factor 2.5 for $\tau = 0.1$. The effect of the charm quark mass is, as expected, also largest for smaller τ. The charm contribution is about 30% for $\tau = 100$ and 10% for $\tau = 1$, which should be compared with 40% for zero mass charm quarks.

We note in particular that also the one-pomeron result satisfies geometric scaling, even down to $\tau = 0.1$. Thus the scaling feature alone is not enough to prove the existence of

JHEP04(2007)067

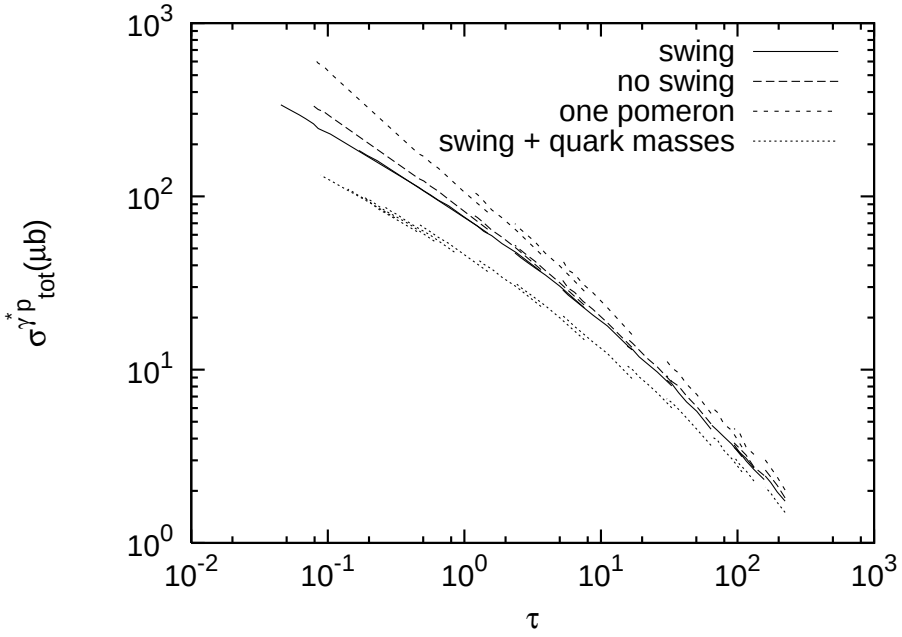

Figure 2: The top three curves show the $\gamma^* p$ total cross section obtained from our Monte Carlo simulation for Q^2 ranging from 0.75GeV^2 to 90GeV^2 and for zero quark mass for 4 flavours. The solid lines show the results for evolution including the dipole swing and also multiple collisions, the long-dashed lines show the results without the swing but including multiple collisions, while the short-dashed lines are results without the swing and also without multiple collisions. It is seen that all three results satisfy geometric scaling. The bottom curve represents our full results shown in figure 1.

saturation. The scale-breaking effect from the charm contribution will be further discussed in section 6. The dominance of the light quark contributions, and the strong correlation between Q^2 and x due to the limited HERA energy, imply that this effect is not so evident in the results shown in figures 1 and 2, although we can see a small shift between the curves for different Q^2 in figure 2.

Although saturation reduces the result for $\tau < 0.5$, there is a more clear break in the experimental data. We note, however, that the experimental points, which show this break, all correspond to small Q^2-values below $0.5\,\text{GeV}^2$. Here we expect also non-perturbative effects to be important. The wave functions in eq. (2.1) extend to very large transverse separations r, and such large dipoles must be suppressed by confinement effects. We also note that energy limitations imply that for fixed Q^2 the experimental points lie in a rather small x-interval, which implies that the points for different Q^2 have a limited overlap. The scaling features for small Q^2 will be further discussed in section 7.

5. Understanding geometric scaling in the linear evolution

The saturation model gives a motivation for geometric scaling in the kinematic range $Q^2 < Q_s^2$, but it does not give a reason for the observed scaling behaviour for $Q^2 > Q_s^2$ at experimentally feasible energies at current accelerators. The arguments in ref. [6] imply

JHEP04(2007)067

that the cross section should scale as a function of $Q^2/Q_s^2(x)$ within a wide kinematic region,

$$1 \lesssim \ln(Q^2/Q_s^2) \ll \ln(Q_s^2/\Lambda_{QCD}^2), \tag{5.1}$$

which is dominated by BFKL diffusion. Here $Q_s^2(x)$ is defined as the scale where the scattering probability is of order 1. As mentioned in the introduction this is a consequence of the fast growth towards small x and wide diffusion to large $k_\perp$ in the leading log BFKL evolution. Both these effects are strongly damped by non-leading effects [7], which therefore reduce the region dominated by linear BFKL evolution. (We also note that both references [7] and [6] point out that with a running coupling the BFKL evolution leads to a saturation scale which satisfies $\ln Q_s^2 \sim \sqrt{Y}$ rather than $\ln Q_s^2 \sim Y$.) For larger Q^2, $k_\perp$-ordered evolution should be dominant and Kwieciński and Staśto [8] have assumed that DGLAP evolution is applicable in the whole region $Q^2 > Q_s^2$, with scaling initial conditions at $Q^2 = Q_s^2$. They then found that although not perfectly scaling, the result showed approximate scaling in the same kinematical domain specified by eq. (5.1). Their arguments do, however, not explain the shape of the saturation line.

We will below argue that scaling is expected both in the region dominated by BFKL diffusion and in the $k_\perp$-ordered double leading log (DLL) regime at larger Q^2. (In the DLL regime this is not obvious from the analytic expressions, but follows from a numerical analysis.) Furthermore we find that the transition between the DLL ($k_\perp$-ordered) and BFKL ($k_\perp$-non-ordered) regimes is given by $Q^2 = Q_{\text{limit}}^2 \propto x^{\lambda_{BFKL}}$, where λ_{BFKL} is the exponent in the solution to the BFKL evolution, estimated to be around 0.3. This implies that Q_{limit}^2 is very close to $Q_{s,GW}^2$, leaving only a very small region where the linear BFKL evolution is dominating.

The qualitative features of the QCD evolution at small x are present already in the leading log $1/x$ results, and we will in section 5.1 discuss a toy model describing the BFKL-DLL transition [29]. Non-leading corrections from e.g. energy conservation and a running coupling are important for the quantitative result. In section 5.2 we try to isolate the most important features of the full dipole cascade MC, to get an intuitive picture of geometric scaling in the non-saturated region.

5.1 Leading log approximation

When both $1/x$ and Q^2 are large the gluon distribution is given by ladders which are ordered in $k_\perp$ and where the splitting function is dominated by the $1/z$ pole. This corresponds to the double log approximation, and for a running coupling the gluon density is given by

$$g(x, Q^2) \sim \exp\left(2\sqrt{\alpha_0 \ln\ln Q^2 \ln 1/x}\right), \text{ where } \bar{\alpha}(Q^2) \equiv \frac{\alpha_0}{\ln(Q^2/\Lambda^2)}. \tag{5.2}$$

This expression does not scale exactly with $Q_s^2 \propto x^{-\lambda}$. Neglecting the very slow variation of $\ln\ln Q^2$ the cross section $\sim g/Q^2$ scales with $Q_s^2 \propto \exp(\lambda'\sqrt{\ln 1/x})$, with some parameter λ', and in ref. [30] it is pointed out that the experimental data can be equally well fitted with both these expressions for Q_s. This is also seen in figure 3, which shows the cross section $\sigma^{\gamma^* p} \sim g/Q^2$ *vs.* τ with g from eq. (5.2) and τ defined from eq. (1.2) but with $\lambda = 0.7$.

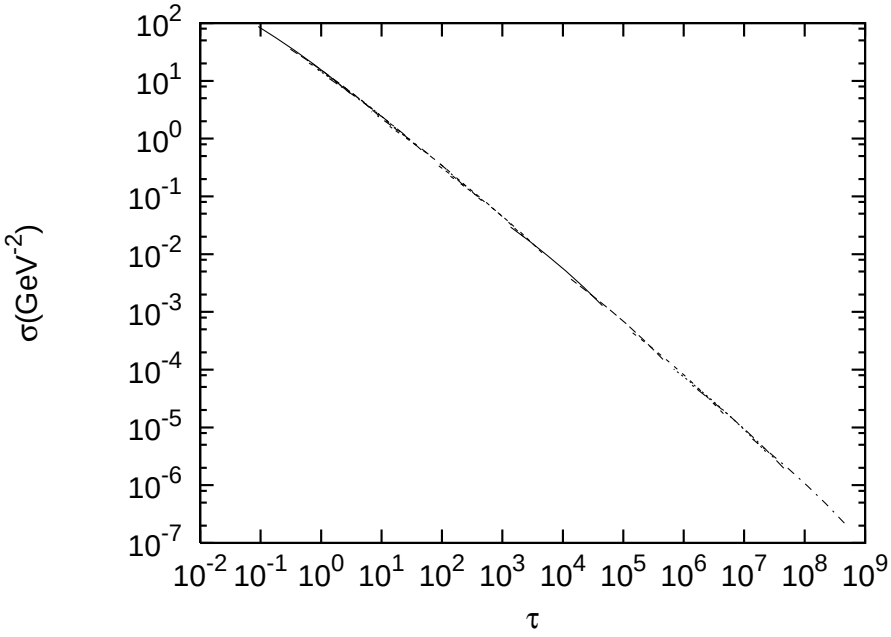

Figure 3: The cross section $\sigma_{\gamma^* p} \sim g/Q^2$ with the gluon density g given by equation (5.2) for different Q^2, varying from $Q^2 = 100\text{GeV}^2$ to $Q^2 = 1.5 \cdot 10^{10}\text{GeV}^2$, and plotted as a function of Q^2/Q_s^2, with Q_s parametrized according to (1.2), but with λ equal to 0.7.

For limited Q^2 we are instead in the BFKL regime dominated by $k_\perp$-non-ordered chains, where the gluon density is growing as a power $1/x^\lambda$ for small x, with λ of the order 0.3. Multiplying by $1/Q^2$ therefore gives directly the scaling cross section

$$\sigma^{\gamma^* p} \sim \frac{Q_s^2}{Q^2} = \tau^{-1} \tag{5.3}$$

with $Q_s^2 \propto 1/x^{0.3}$.

We now also want to argue that, as described in ref. [29], the line $Q^2 = Q^2_{\text{limit}}$ corresponding to the separation between ordered (DGLAP-like) chains and unordered (BFKL-like) chains, is also close to $Q^2_{s,GW}$. In the double log approximation the (non-integrated) gluon distribution G is given by the $k_\perp$-ordered expression

$$G(x,k_\perp^2) \sim \sum_n \prod_i^n \left\{ \int \frac{4\alpha_s}{3\pi} \frac{dk_{\perp,i}^2}{k_{\perp,i}^2} \theta(k_{\perp,i} - k_{\perp,i-1}) \frac{dx_i}{x_i} \theta(x_{i-1} - x_i) \right\} \delta(x - x_n) \delta(k_\perp^2 - k_{\perp,n}^2). \tag{5.4}$$

With the notation $l_i \equiv \ln(1/x_i)$ and $\kappa_i \equiv \ln(k_{\perp,i}^2/\Lambda^2)$ (and $\kappa = \ln(k_\perp^2/\Lambda^2)$, $l = \ln(1/x)$) we get for a fixed coupling the result

$$\begin{aligned} G &\sim \sum_n \left\{ \prod_i^n \int^\kappa \bar{\alpha} d\kappa_i \theta(\kappa_i - \kappa_{i-1}) \cdot \prod_i^n \int^{\ln 1/x} dl_i \theta(l_i - l_{i-1}) \right\} \\ &= \sum_n \bar{\alpha}^n \cdot \frac{\kappa^n}{n!} \cdot \frac{l^n}{n!} = I_0(2\sqrt{\bar{\alpha} \ln Q^2 \ln 1/x}) \sim \exp\left(2\sqrt{\bar{\alpha} \ln Q^2 \ln 1/x}\right). \end{aligned} \tag{5.5}$$

JHEP04(2007)067

For a running α_s we have instead of $dk^2_{\perp,i}/k^2_{\perp,i} = d\kappa_i$ a factor $d\kappa_i/\kappa_i = d\ln\kappa_i$, which then gives the result in eq. (5.2).

In the BFKL region with small x but not so large Q^2, the $k_\perp$-ordered phase space in eq. (5.4) becomes small, and chains which are not ordered in $k_\perp$ give important contributions. The BFKL evolution can be formulated in different ways. Expressed in terms of the primary [20] or backbone [21] gluons a step downwards in $k_\perp$ is suppressed by a factor $k^2_{\perp i}/k^2_{\perp i-1}$ [20, 31]. We note that this implies that a maximum $k_\perp$-value in the chain will contain the factor $dk^2_{\perp\max}/k^4_{\perp\max}$ which can be interpreted as a hard parton-parton subcollision with the expected cross section proportional to $d\hat{t}/\hat{t}^2$. Expressed in the logarithmic variable κ, a step down is consequently suppressed by a factor $\exp(\kappa_i - \kappa_{i-1}) = \exp(-\delta\kappa)$. This implies that the effective range allowed for downward steps corresponds to approximately one unit in κ. Consequently we find that the phase space limits $\kappa_i \gtrsim \kappa_{i-1}$ in eq. (5.5) is replaced by [29, 31]

$$\kappa_i \gtrsim \kappa_{i-1} - 1. \tag{5.6}$$

For a fixed α_s the transverse momentum integrals giving $\kappa^n/n!$ in eq. (5.5) will be replaced by

$$\int_0^\kappa \prod_i^n d\kappa_i \theta(\kappa_i - \kappa_{i-1} - 1) \approx \frac{(\kappa+n)^n}{n!} \tag{5.7}$$

When κ is very large we recover the DLL result in eq. (5.5), but for smaller values of κ we find instead using Stirling's formula

$$\kappa \text{ small } \Rightarrow \frac{(\kappa+n)^n}{n!} \sim \frac{n^n}{n!} \sim e^n \tag{5.8}$$

which implies

$$G \sim \sum_n \frac{[\bar{\alpha}\, e \ln(1/x)]^n}{n!} = e^{e\,\bar{\alpha}\ln(1/x)} = \frac{1}{x^\lambda} \tag{5.9}$$

with

$$\lambda = e\,\bar{\alpha} \approx 2.72\,\bar{\alpha}. \tag{5.10}$$

In this range the chain corresponds to a random walk in $\ln k^2_\perp$. The result should be compared with the result from the leading order BFKL equation, which gives

$$\lambda = 4\ln 2\,\bar{\alpha} \approx 2.77\,\bar{\alpha}. \tag{5.11}$$

We see that this simple picture describes the essential features of BFKL evolution.

We note here in particular that the boundary between the domains dominated by $k_\perp$-ordered chains (eq. (5.5)) and $k_\perp$-non-ordered chains (eq. (5.8)) is determined by the relation

$$\ln k^2_{\perp\text{limit}} = e\,\bar{\alpha}\ln(1/x). \tag{5.12}$$

We see that if we replace the LL λ-value by a lower value ≈ 0.3, as indicated by the experimental data, then $k^2_{\perp\text{limit}}$ is similar to $Q^2_{s,GW}(x)$ from the early fit by Golec-Biernat and Wüsthoff [2, 3]. This shows that the line $Q^2 = Q^2_{s,GW}(x)$ (corresponding to $\tau = 1$) is actually close to Q^2_{limit}, which represents the separation between $k_\perp$-ordered (DGLAP-like) chains and non-ordered (BFKL-like) chains.

5.2 The dipole cascade

The qualitative features in the LLA in section 5.1 are modified by energy conservation and other non-leading effects. We will here study how the scaling behaviour can be seen in the dipole cascade model presented in section 3, trying now to isolate the most important features of the full MC simulation.

Let us look at a dipole with size r, which after a rapidity interval Δy splits in two dipoles with sizes $r_>$ and $r_<$, with $r_>$ larger than $r_<$. Figure 4 shows the MC results for the average values of the ratios $r_>/r$ and $r_</r$ for different values for the "time", Δy, it takes from the formation of the dipole till it splits. The probability distribution $dP/d\Delta y$ is also shown. We see here that a dipole typically splits in two dipoles, where one has the same size as the parent while the other has just half its size. This result is independent of the step Δy and of the photon virtuality Q^2. This also shows that it is independent of the size of the parent dipole. We note that these results depend crucially on the energy-momentum conservation in the evolution. Without this constraint the typical splitting would occur within a very small rapidity step giving one virtual dipole with a size close to the necessary cutoff. When the cutoff goes to zero both Δy and $r_</r$ would also go to zero. Essential for the simple result in figure 4 is the conservation of both p_+ and p_-. This is seen in figure 5, which shows the corresponding result obtained with only p_+-conservation.

Let us then assume that each dipole r splits after a typical Δy, which from the distribution $dP/d\Delta y$ is found to be around 1.8 units, into two dipoles with sizes r and r/a, with the parameter a of the order of 2. If Y denotes the total rapidity range the number of steps will be $N = Y/\Delta y$ and the number of dipoles $2^N = 2^{(Y/\Delta y)}$. Starting from an initial dipole r_0 the number of dipoles having size r_0/a^n will be equal to $\binom{N}{n}$, with $n = 0, 1, \ldots, N$.

To study the scaling behaviour of the $\gamma^* p$ cross section within this approximation, we can treat the photon as a dipole with size $r_\gamma = 1/Q$. In the linear region the initial proton can also be treated as a single dipole with size $r_p = 1/\Lambda$. The cross section for the scattering of two dipoles, r_1 and r_2, is given by [17]

$$\sigma_{dd}(r_1, r_2) = 2\pi\alpha_s^2 r_{\min}^2 \{1 + \ln(\frac{r_{\max}}{r_{\min}})\} \tag{5.13}$$

where $r_{\max}$ ($r_{\min}$) is the largest (smallest) of the two colliding dipoles r_1 and r_2. We study the collision in a frame where only the proton is evolved, and the photon therefore treated as a single dipole.

When Q is larger than $a^N \cdot \Lambda$ the photon dipole is smaller than all dipoles in the proton cascade. The resulting cross section is then given by

$$\begin{aligned}\sigma^{\gamma^* p}(Q^2, Y) &= 2\pi\alpha_s^2 \sum_{n=0}^{N} \binom{N}{n} Q^{-2} \left\{1 + \ln\left(\frac{Q}{a^n \Lambda}\right)\right\} \\ &= \pi\alpha_s^2 Q^{-2} 2^N \left\{2 - N \ln a + \ln\frac{Q^2}{\Lambda^2}\right\} \propto \frac{Q_{sc}^2}{(\Lambda^2 Q^2)} \left\{1 + \frac{1}{2}\ln\left(\frac{Q^2}{Q_{sc}^2}\right)\right\}, \end{aligned} \tag{5.14}$$

where in the last expression we have used $a = 2$, $N = Y/\Delta y$ and $Q_{sc}^2 = \Lambda^2 x^{-\ln 2/\Delta y} \approx \Lambda^2 x^{-0.38}$. The result is obviously scaling, and the exponent 0.38 is not far from the experimental fit around 0.3. We note also that in this case the dominating contribution

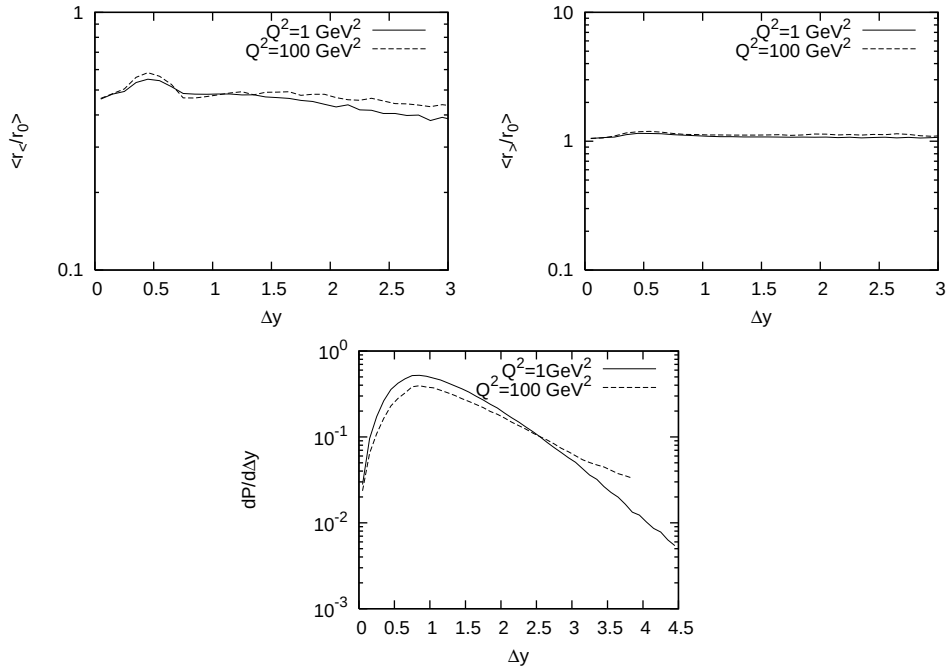

Figure 4: The top figures show how the average values of the ratios $r_</r_0$ (left) and $r_>/r_0$ (right) for splitting events vary with the rapidity separation Δy. It is seen that both these ratios are approximately constant independent of Δy, and that $r_>/r_0$ is ≈ 1. The bottom figure presents the Δy-distribution $dP/d\Delta y$. This distribution has a peak around $\Delta y = 1$ and falls off exponentially for larger Δy-values.

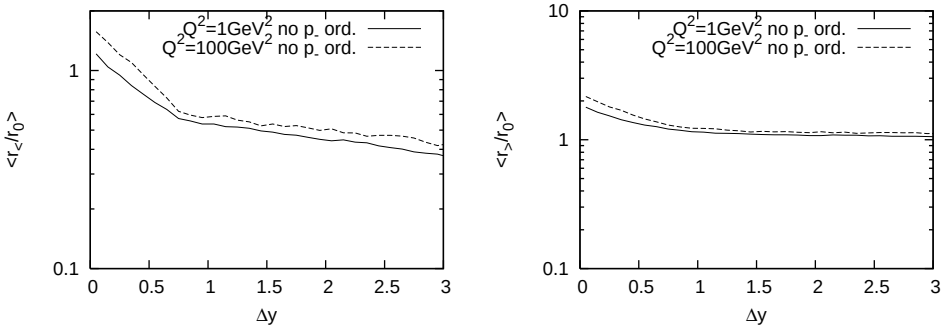

Figure 5: The averaged ratios $\langle r_</r_0\rangle$ and $\langle r_>/r_0\rangle$ as functions of Δy in a simulation where p_- is not conserved in the evolution. We see that p_+-conservation is not enough to get the almost constant ratios seen in figure 4.

comes from dipole chains where the dipoles are ordered in size and where the last dipole in the cascade is larger than the photon dipole. This just corresponds to the dominance of $k_\perp$-ordered DGLAP-type ladders.

For smaller Q-values the curly bracket in eq. (5.14) overestimate the contribution from small proton dipoles represented by n-values for which $a^n \cdot \Lambda > Q$. The largest terms in the sum are obtained when the binomial factor has its maximum, i.e. for $n \approx N/2$. Therefore the result in eq. (5.14) is a good approximation as long as $Q > a^{N/2} \cdot \Lambda$. Indeed, using

JHEP04(2007)067

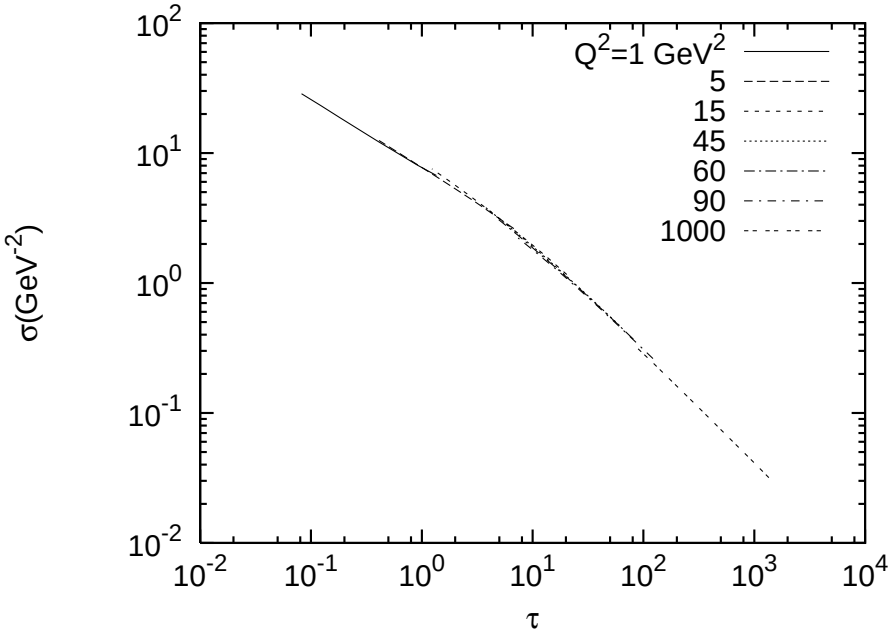

Figure 6: The toy model cross section in (5.15) plotted as a function of the scaling variable with $Q_{sc}^2 = \Lambda^2 \cdot x^{-0.4}$, with $\Lambda^2 = 0.1\text{GeV}^2$, and for different Q^2. The normalization here is not of interest and all prefactors has been simply put to 1. We indeed see that the result shows scaling, for low and high Q^2 alike.

Stirling's formula we can write $\binom{N}{N/2} \approx 2^N$, and in the saddlepoint approximation we again arrive at the result given in eq. (5.14). We note that the constraint $Q > a^{N/2} \cdot \Lambda$ corresponds just to $Q^2 > Q_{sc}^2$, which thus is the limit for the dominance of $k_\perp$-ordered, DGLAP-type evolution chains.

Below this region, i.e. for $Q^2 < Q_{sc}^2$, it is not a good approximation to neglect the contributions from scatterings where the proton dipoles are smaller than the photon dipole. The full expression, including all contributions, can be written as

$$\sigma^{\gamma^* p}(Q^2, Y) \propto \sum_{n=0}^{m} \binom{N}{n} Q^{-2} \left\{ 1 + \ln\left(\frac{Q}{a^n \Lambda}\right) \right\} + \sum_{n=m+1}^{N} \binom{N}{n} a^{-2n} \Lambda^{-2} \left\{ 1 + \ln\left(\frac{a^n \Lambda}{Q}\right) \right\} \tag{5.15}$$

where $m \equiv \frac{\ln Q/\Lambda}{\ln a}$. This expression is more complicated, but we show in figure 6 the result of a numerical evaluation expressed with a scale $Q_{sc}^2 \propto x^{-0.4}$. We see that scaling is indeed satisfied for a large range of values for Q^2, also in the kinematic region dominated by chains which are not well ordered in dipole size or in transverse momentum.

We note that our toy model has important similarities with the empirical model presented in ref. [32]. In this paper it is demonstrated that geometric scaling follows from an assumption that the dipole cascade in the proton is dominated by dipoles with size Q_s^{-1} (while the virtual photon can be represented by a dipole with size Q^{-1}). Our toy model approximation of the full MC cascade has just this feature; the dipole multiplicity is given by the binomial coefficient $\binom{N}{n}$, with a maximum for $n = N/2$ corresponding to $r = 1/Q_{sc}$.

JHEP04(2007)067

The result in eq. (5.14), which is obtained for $Q > Q_{sc}$ using the saddlepoint approximation, is thus identical to the corresponding result in [32]. Ref. [32] also points out that if events with $Q < Q_s$ can be described by an analogous cascade evolution of the initial photon dipole, then the expression $Q/Q_s\sigma^{\gamma^* p}(Q/Q_s(x))$ is symmetric under the exchange $Q \leftrightarrow Q_s(x)$. This symmetry was initially observed in the HERA data by ref. [1]. For these smaller Q-values ($Q < Q_{sc}$) the dominant contributions from $n \approx N/2$ are contained in the second term in eq. (5.15). Using again the saddlepoint approximation we also obtain the symmetric result

$$\sigma^{\gamma^* p}(Q^2, Y) \approx 2\pi\alpha_s^2 2^N a^{-N}\Lambda^{-2}\left\{1 + \ln\left(\frac{a^{N/2}\Lambda}{Q}\right)\right\} \approx 2\pi\alpha_s^2\Lambda^{-2}\left\{1 + \ln\left(\frac{Q_{sc}}{Q}\right)\right\}. \quad (5.16)$$

In conclusion we find that $Q^2 = Q_{sc}^2 \propto x^{-\lambda}$, with λ approximately equal to the BFKL exponent, specifies the limit between dominance of $k_\perp$-ordered and $k_\perp$-non-ordered chains, and that a simple toy model having this property gives the qualitative features of the scaling dynamics for both large and small τ. We also see that the toy model approximation to the full MC simulation of the dipole cascade model have important similarities with the empirical model in ref. [32], and gives a scaling result with a scaling exponent not far from what is observed at HERA.

6. Scaling features in the charm contribution

It is well known from HERA data that charm quarks contribute a significant part to the total cross section. As discussed in section 4, the large charm quark mass modifies the scaling properties, and it is seen that the HERA charm data do indeed not scale as a function of $\tau = Q^2/Q^2_{s,GW}(x)$. As pointed out in ref. [33] they do, however, scale quite well as a function of the modified scaling variable $\tau_c = (Q^2 + 4m_c^2)/Q_s^2$

From the photon wave function in (2.1) we see that the term proportional to the Bessel function K_1^2 in $|\psi_T|^2$ only contains Q^2 and m_f in the combination $z(1-z)Q^2 + m_f^2$. If z-values around 1/2 dominate, we would expect that the charm contribution is gradually switched off when Q^2 is of the order $4m_c^2$ or smaller, which necessarily leads to a breaking of geometric scaling. The sum of the terms proportional to K_0^2 in $|\psi_T|^2$ and $|\psi_L|^2$ is proportional to $[4z(1-z)]z(1-z)Q^2 + m_f^2$, and for z close to 1/2 the square bracket equals 1, and we get the same factor $z(1-z)Q^2 + m_f^2$ as before. From these features we may expect that the charm contribution scales approximately with a modified scaling parameter where, for example, we replace Q^2 by $Q^2 + n{\cdot}m_c^2$ in the definition of τ, for some number n which should be close to or a little larger than 4.

In figure 7 we show data for the charm cross section from ZEUS [34] and our MC obtained for $m_c = 1.4\,\mathrm{GeV}$. In this figure we have used the scaling variable

$$\tau_c = (Q^2 + 6m_c^2)/Q^2_{s,GW}(\bar{x}) \quad \text{with} \quad \bar{x} = (Q^2 + 6m_c^2)/W^2, \quad (6.1)$$

obtained with $n = 6$ in the definition of τ_c, which we find gives somewhat better scaling properties. This implies that $\tau_c = (1 + 6m_c^2/Q^2)^{1+\lambda}{\cdot}\tau_{GW}$. We here first note that the MC

JHEP04(2007)067

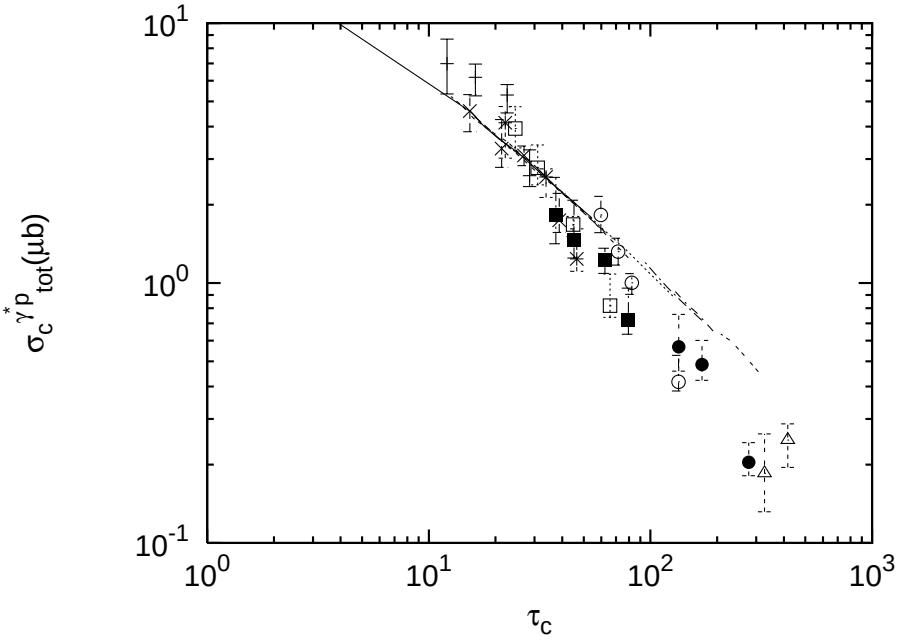

Figure 7: The total charm cross section, $\sigma_T^c + \sigma_L^2$ plotted as a function of τ_c defined in (6.1) with $\lambda = 0.35$ and $m_c = 1.4\,\mathrm{GeV}$. Results are shown for Q^2 between 2 and $130\,\mathrm{GeV}^2$. We see that the result scales fairly well with this scaling parameter. Data points are taken from ref [34].

agrees quite well with the data, being only a little high for the largest τ-values. Secondly we confirm the observation in ref. [33] that the charm cross section does scale well as a function of such a modified scaling variable.

The value $n = 6$ chosen for the scaling variable in eq. (6.1) is not crucial for the scaling behaviour, which works rather well also for $n = 4$. We note, however, that replacing x by $\bar{x}$ in Q_s only contributes a minor part to the difference between τ_c and τ_{GW}, represented by the factor $(Q^2 + 6m_c^2)^\lambda$. More important is the replacement $Q^2 \to Q^2 + 6m_c^2$ in eq. (6.1). This is illustrated in figure 8, which shows that scaling does not hold if we replace τ by $Q^2/Q^2_{s,GW}(\bar{x})$.

We want here to point out that the effect of the charm mass is reduced very slowly for larger Q^2. Integrating over the dipole size, $\mathbf{r}$, we obtain from a dimensional analysis

$$\int d^2\boldsymbol{r} K_i^2(\epsilon r)\sigma(z,\boldsymbol{r}) \propto \frac{1}{\epsilon^4}\,, \qquad \epsilon = \sqrt{z(1-z)Q^2 + m_f^2}. \tag{6.2}$$

When $4Q^2$ is small compared to m_f^2 we have $\epsilon \approx m_f$, and the charm cross section ought to scale as

$$\sigma_T \propto \frac{1}{m_c^2}, \qquad \sigma_L \propto \frac{Q^2}{m_c^4}. \tag{6.3}$$

We see here that the longitudinal contribution depends on two separate scales Q^2 and m_c^2. In the other limit, when $z(1-z)Q^2 > m_c^2$ we can neglect m_c. However, since $z(1-z)$ can take on arbitrarily small values for fixed Q^2, we the effect of the charm mass can be

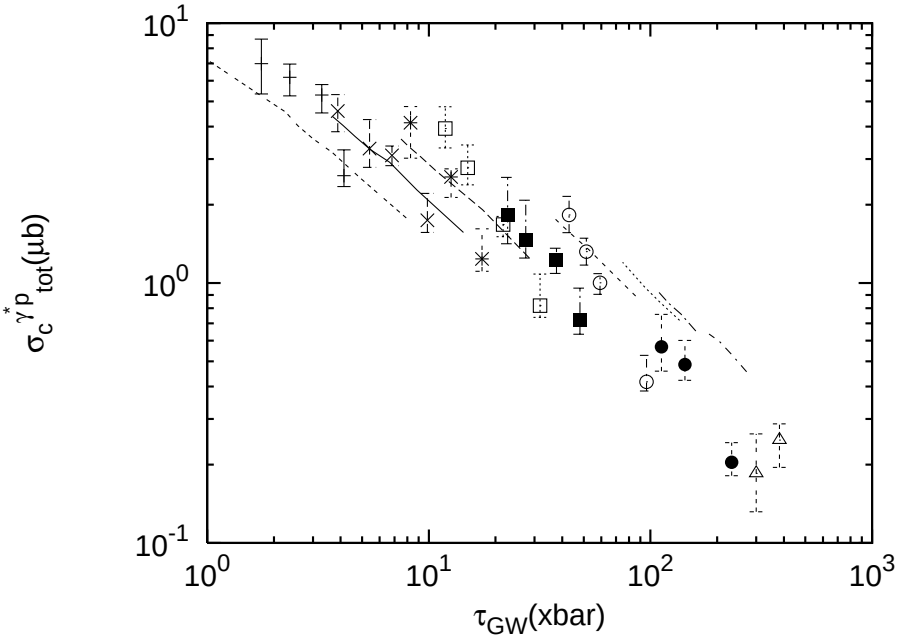

Figure 8: Here we plot the charm cross section as a function of $Q^2/Q_s^2(\bar{x})$ with the same parameters as in figure 7. In this case we see that the result does not scale, which shows the importance of replacing Q^2 with $Q^2 + n \cdot m_c^2$, $n \sim 4$, as argued in the text.

important also for high Q^2. In the MC results presented in figure 7 the reduction due to the charm mass is about 30% for $Q^2 = 90\,\mathrm{GeV}^2$ and 55% for $Q^2 = 15\,\mathrm{GeV}^2$. This slow decrease of the mass effect is also seen in figure 2. (We should here also remark that the transverse wave function ψ_T is not normalizable due to the singularity $K_1^2(r) \sim 1/r^2$ at small r. However, at small r the dipole-proton cross section behaves like r^2 and thus the result is still finite.)

7. Interaction at smaller Q^2

Due to the limited energy in the HERA accelerator the experimental data in the region $\tau < 0.5$ are all obtained for rather small virtualities Q^2, where non-perturbative effects must be expected.

7.1 Can the perturbative dipole formalism be used for Q^2 below $1\,\mathrm{GeV}^2$?

For small Q^2 the wave functions in eq. (2.1) extend to very large transverse separations r, and such large dipoles must be suppressed by confinement effects. The interaction of these photons is usually described in terms of two separate components, a vector dominance contribution and a direct coupling to the quarks. We will here test if it is possible to represent the interaction of these photons with a finite mass for the light quarks, which effectively suppresses the contribution from the very large dipoles. Because the contribution from the strange quark is suppressed by its smaller electric charge, and therefore relatively small, it is not possible to study in any detail the effect of the strange quark mass. We

JHEP04(2007)067

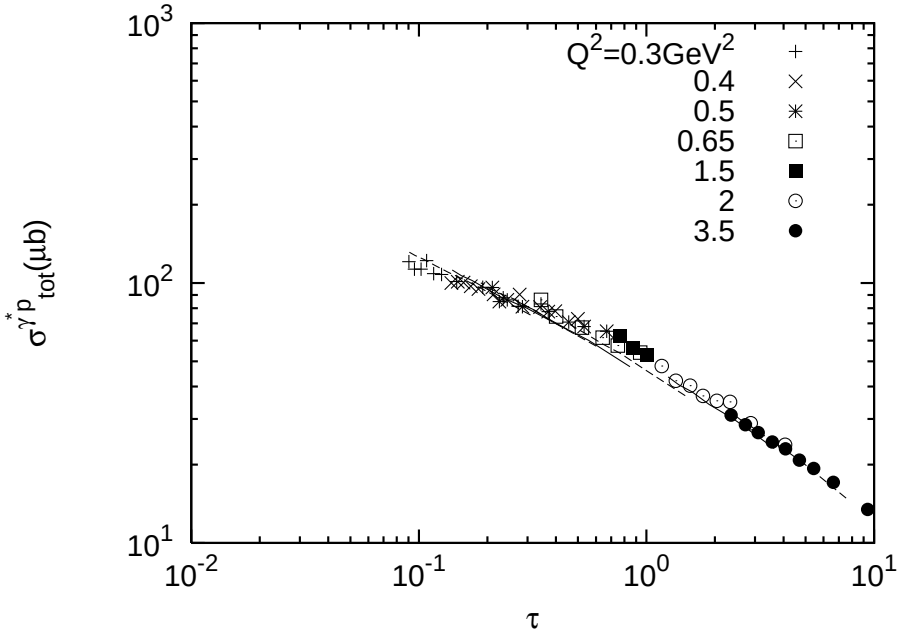

Figure 9: The $\gamma^* p$ total cross section plotted as a function of the scaling variable τ for low Q^2 values. Points are data from the H1 [27] and ZEUS [28] collaborations, while the lines are results obtained from our Monte Carlo. We can here see a successive suppression of the cross section for smaller Q^2 as a result of the finite quark masses.

therefore use a single quark mass, m_l, for all the light quarks, u, d, and s. The results in figure 9 for Q^2 in the range 0.3-3.5 GeV^2 are obtained for $m_l = 60$MeV and $m_c = 1.4$GeV, and we here show the model results for the same combinations of x- and Q^2-values as in the experimental data. We see that the experimental data are very well reproduced by the model calculations, which gives some support to the application of this perturbative description also for these small virtualities.

The effective quark mass is quite small, and we would have expected a larger suppression for small Q^2. The value 60 MeV is smaller than Λ_{QCD}, and also smaller than the effective mass obtained in ref. [35] in an analysis of the vector-current two-point function. Ref. [35] studies a model with an effective quark mass which varies with Q^2, becoming smaller when Q^2 is increased. The agreement in figure 9 would actually be improved by such a varying effective mass, but we do not believe that the accuracy of our model is sufficient to claim that this improvement is significant. We have therefore here only used a constant effective quark mass in the wave functions in (2.1).

7.2 Is geometric scaling obeyed for $Q^2/Q_s^2 < 1$?

The effect of a finite quark mass is approximately a multiplicative factor which suppresses the cross section for smaller Q^2. As discussed in section 6 the result of the quark mass in the photon wave functions corresponds roughly to a suppression by a factor $Q^2/(Q^2 + 4m_f^2)$. The fact that the model results in figure 9 look as a scaling function is therefore a consequence of the strong correlation between x and Q^2 in the experimental data. The finite

JHEP04(2007)067

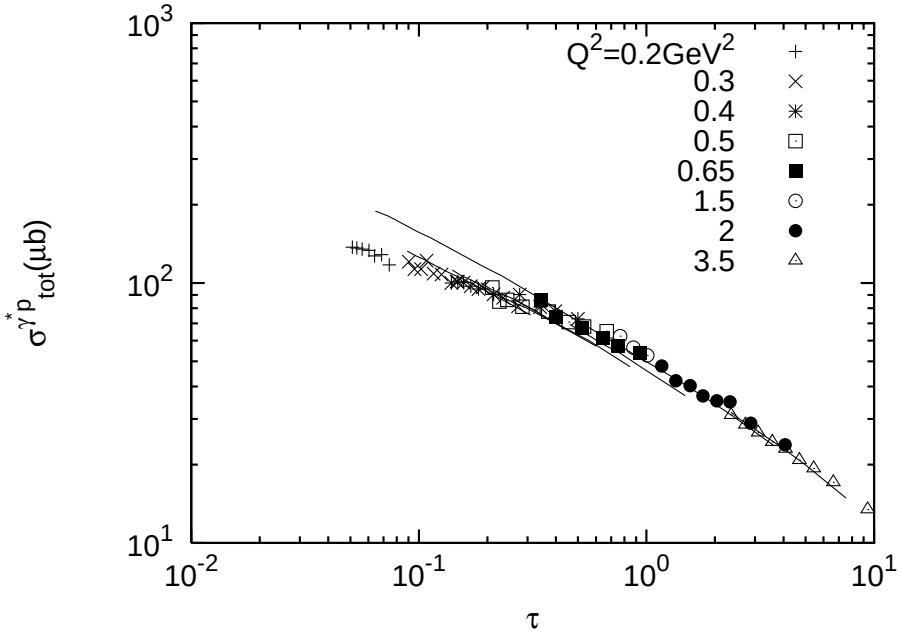

Figure 10: In this figure we extend the result for $Q^2 = 2\text{GeV}^2$ to smaller τ-values. We can here see a deviation from the scaling behaviour at higher energies, about a factor 1.4 for $\tau \approx 0.07$ corresponding to $x \approx 3 \cdot 10^{-9}$ for $Q^2 = 2\text{GeV}^2$. In this plot the deviation from the scaling curve is to a large extent due to the effective light quark mass.

energy in the HERA accelerator implies that for small values of τ there are only data for (x, Q^2)-values within a very small interval. With a future accelerator with higher energy, one could also reach smaller τ-values keeping $Q^2 > 1\text{GeV}^2$. For these Q^2 we do not get much suppression from the light quark masses, and figure 10 shows that the scaling curve will lie somewhat above the present HERA results. In the figure we show the extend the curve for $Q^2 = 2\text{GeV}^2$ to $\tau \approx 0.07$. As can be seen, the difference is increasing for smaller τ-values and is about a factor 1.4 for $\tau \approx 0.07$. We also expect to see the scalebreaking effects of the charm mass for $1\text{GeV}^2 \lesssim Q^2 \lesssim 10\text{GeV}^2$, while for higher Q^2 these effects should be gradually switched off. This cannot, however, be observed at accelerators in the foreseeable future.

As a conclusion of this section we predict that at higher energies the data will scale at larger values for the cross section than the present HERA data for $\tau < 1$. We should, however, point out that the analysis in this section only holds for the particular value $\lambda = 0.3$ for the saturation scale in eq. (1.2). For a different λ the scaling behaviour will be different and it turns out that the deviation from the scaling behaviour would be somewhat reduced with a higher λ.

8. Impact parameter dependence of the traveling wave

In this section we will look at the impact parameter dependence of the dipole-proton scattering amplitude $T^{dp}(b)$, defined as $T = 1 - S$. We expect that the contribution from

small dipoles is reduced for large impact parameters, which may result in different scaling behaviour for central and peripheral collisions. This feature may be of special interest in studies of diffraction.

The amplitude T^{dp} is related to the total dipole-proton cross section by the relation

$$\sigma^{dp}(z,\boldsymbol{r}) = 2\int d^2\boldsymbol{b}\, T^{dp}(b). \tag{8.1}$$

To get the amplitude for photon-proton scattering, the amplitude $T^{dp}(b)$ has to be weighted by the photon wave function in eq. (2.1). The average value $\langle T\rangle$ will then depend on the virtuality Q^2 and the impact parameter b.

In the introduction we mentioned the similarity between the high energy evolution equations for T and a certain type of equation (or rather a class of equations) from statistical physics, known as the FKPP equation. Neglecting the impact parameter dependence, the BK equation for the amplitude $T(l,Y)$ (with $l \equiv \ln k^2$) is analogous to the FKPP equation for the function $u(x,t)$, with the identifications $l \leftrightarrow x$ and $\bar{\alpha}Y \leftrightarrow t$. The asymptotic solution, as $t \to \infty$, $u_{as}(x,t) = u(x-vt)$, then corresponds to $T_{as}(l,Y) = T(l-\lambda Y)$ in QCD. If we define $Q_s^2 = \exp(\lambda Y)$ as before the solution satisfies the geometric scaling relation $T(l,Y)_{as} = T(\ln k^2/Q_s^2)$. There are a number of conditions which must be satisfied in order to obtain an asymptotic solution of this form, and for a short review on traveling wave solutions in QCD we refer to [36].

As our model satisfies geometric scaling we can expect that the function $\langle T\rangle(\ln Q^2)$ plotted for different Y-values looks like a traveling wave. This can be seen in figure 11 which shows results for $Y = 6, 8, 10$ and 12. In this figure we also show the result for different impact parameters b. If we look at different points with the same $\langle T\rangle$-value, the velocity is determined by the relation

$$v(b) = \frac{\Delta \ln Q^2}{\Delta Y} \tag{8.2}$$

The results in figure 11 correspond to the following velocities when saturation effects are included in the amplitude: $v(b=0) = 0.28$, $v(b = 0.5fm) = 0.35$ and $v(b = 1fm) = 0.37$. (For the one pomeron amplitude we instead obtain $v(b=0) = 0.41$, $v(b = 0.5fm) = 0.46$ and $v(b = 1fm) = 0.48$) Thus the velocity varies significantly with the impact parameter, being smaller for central collisions and larger for peripheral collisions. As the scattering probability is largest for the central collisions, these results seem to be reasonably consistent with weighted average over impact parameters corresponding to the velocity $v \approx 0.3$ observed for the total cross section.

In figure 11 we can see that also the one pomeron amplitude, which contains no saturation effects, seems to exhibit the form of a traveling wave. We also see that we need quite high energies, corresponding to $x \approx 6 \cdot 10^{-6}$ for $Q^2 \approx 4\text{GeV}^2$ and $b = 0$, before the one pomeron amplitude reaches the unitarity limit $T = 1$. However, it is also seen that saturation effects reduce the amplitude by about 10% for larger Q^2 and about 40% for small $Q^2 \sim 1\text{GeV}^2$ already at $x \sim 10^{-3}$ for $b = 0$. This result is consistent with the previous results presented in figure 2.

JHEP04(2007)067

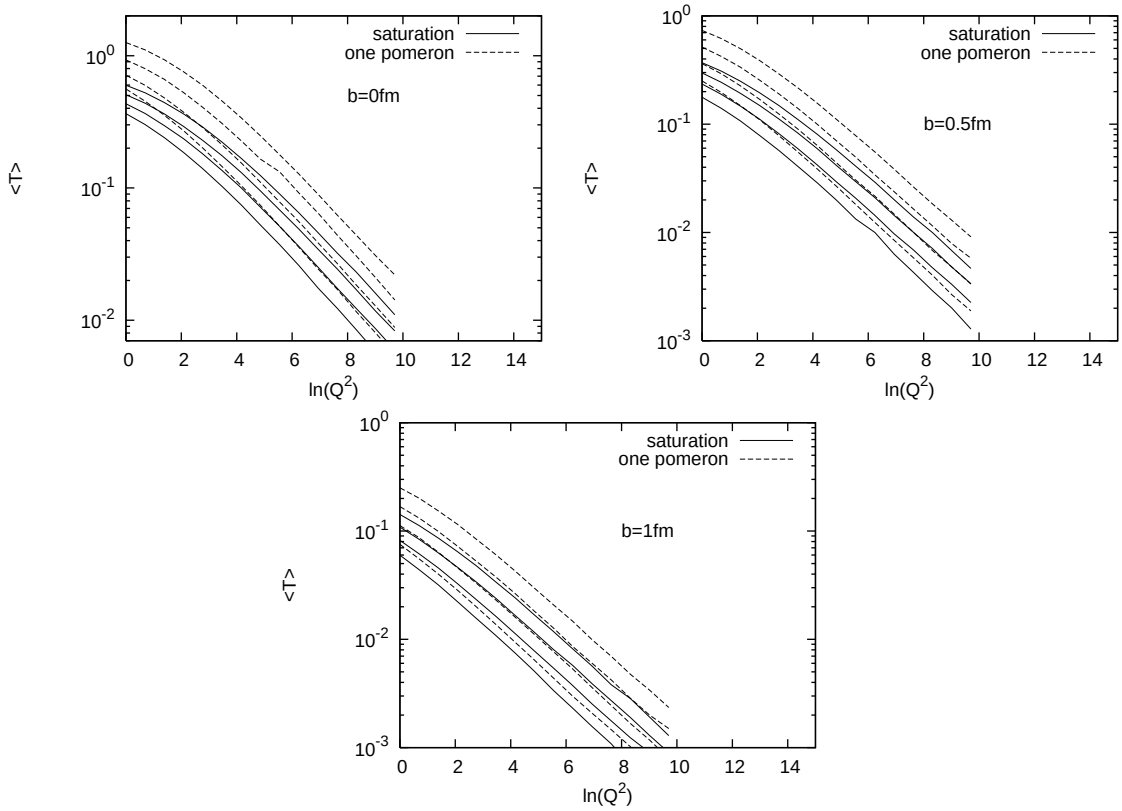

Figure 11: The average scattering amplitude as a function of $\ln(Q^2/1\text{GeV}^2)$ for $Y = 6, 8, 10$ and 12 and impact parameters $b = 0, 0.5, 1$fm. Both the amplitude containing full saturation effects and the linear one pomeron amplitude are shown. For the amplitude including saturation we obtain from here the velocities $v(b = 0) = 0.28$, $v(b = 0.5fm) = 0.35$ and $v(b = 1fm) = 0.37$.

9. Conclusions

DIS data from HERA show a striking regularity as $\sigma^{\gamma^* p}$ is a function of the ratio $\tau = Q^2/Q_s^2(x)$ only, with $Q_s^2(x)$ given by eq. (1.2) [1–3]. Such a geometric scaling has been expected in the range $\tau < 1$, as a natural consequence of saturation when the gluon density becomes very high, and there has been a lot of discussion in the literature whether saturation has or has not been observed at HERA. Modifications of the saturation model including DGLAP evolution [4] improves the agreement with data for larger Q^2, but it has not been equally obvious how geometric scaling follows in a natural way from QCD evolution in the non-saturated domain. The traveling wave solutions to the nonlinear evolution equations in QCD do predict geometric scaling also for $\tau > 1$ [9, 10], but these solutions are valid only at extremely high energies, far beyond what is available at the HERA accelerator.

In this paper we have tried to shed some light on these questions: What is the reason for scaling for $\tau > 1$, and is saturation indeed the reason for geometric scaling for $\tau < 1$? Supporting the saturation idea is the fact that the scaling curve seems to have a break

just around $\tau = 1$. There are, however, also other effects which contribute to a break in this region. In ref. [29] it is shown that the transition between $k_\perp$-ordered (DGLAP-like) chains and $k_\perp$-non-ordered (BFKL-like) chains is expected close to Q_s^2. Secondly the finite energy in the HERA machine implies that experimental data for $\tau < 1$ are only available for $Q^2 < 1\text{GeV}^2$, where nonperturbative effects begin to be important.

To study the influence on the scaling from different dynamical effects we have used the dipole cascade model presented in ref. [14]. This model is based on Mueller's dipole cascade model, but includes energy-momentum conservation and saturation effects, not only from multiple subcollisions but also from pomeron mergings in the cascade evolution, and it does successfully reproduce the data from HERA.

Our conclusion is that scaling is a natural consequence of the dipole evolution in the linear region $\tau > 1$. Indeed, neglecting saturation the linear evolution exhibits geometric scaling at high energies for τ-values both larger and smaller than 1. The change from the DGLAP to the BFKL regime causes a change in the slope of the scaling curve, but this change is rather smooth, without a sharp break at $\tau = 1$. The break seen in the HERA data is to a significant part caused by saturation, but to an even larger extent by scalebreaking effects at low Q^2. The latter are partly due to the large c-quark mass and partly due to non-perturbative effects related to confinement for the light u-, d-, and s-quarks. Therefore we predict that the results from a future higher energy machine will show deviations from the scaling behaviour in the variable τ_{GW}. These results are expected to lie above the HERA results for $\tau_{GW} < 1$, and be represented by a curve which is more smooth around $\tau_{GW} = 1$. (Recently it has also been predicted that a new type of scaling, called diffusive scaling, will occur at very high energies, but we have in this paper concentrated on energies which might be within reach at some future accelerator.)

We study the charm contribution separately, and compare with data for the charm cross section. The charm contribution does not scale as the total cross section, but we see that it does scale rather well as a function of the variable $(Q^2 + 6m_c^2)/Q_s^2(\bar{x})$. Finally we have studied how the scaling feature varies with impact parameter. We here see that the effective power λ in (1.2) is somewhat smaller for central collisions and larger for peripheral collisions, averaging out to the observed value around 0.3. Such a variation may be of interest in studies of diffractive scattering.

Acknowledgments

We want to thank Leif Lönnblad for valuable discussions and help with the MC simulation. We are also grateful to Hannes Jung for pointing out to us the lack of scaling in the charm contribution, and to Edmond Iancu for useful comments on the manuscript.

References

[1] A.M. Stasto, K. Golec-Biernat and J. Kwiecinski, *Geometric scaling for the total γ^* p cross-section in the low x region*, *Phys. Rev. Lett.* **86** (2001) 596 [hep-ph/0007192].

[2] K. Golec-Biernat and M. Wusthoff, *Saturation effects in deep inelastic scattering at low Q^2 and its implications on diffraction*, *Phys. Rev.* **D 59** (1999) 014017 [hep-ph/9807513].

[3] K. Golec-Biernat and M. Wusthoff, *Saturation in diffractive deep inelastic scattering*, *Phys. Rev.* **D 60** (1999) 114023 [hep-ph/9903358].

[4] J. Bartels, K. Golec-Biernat and H. Kowalski, *A modification of the saturation model: DGLAP evolution*, *Phys. Rev.* **D 66** (2002) 014001 [hep-ph/0203258].

[5] K. Golec-Biernat and S. Sapeta, *Heavy flavour production in dglap improved saturation model*, *Phys. Rev.* **D 74** (2006) 054032 [hep-ph/0607276].

[6] E. Iancu, K. Itakura and L. McLerran, *Geometric scaling above the saturation scale*, *Nucl. Phys.* **A 708** (2002) 327 [hep-ph/0203137].

[7] K. Golec-Biernat, L. Motyka and A.M. Stasto, *Diffusion into infra-red and unitarization of the bfkl pomeron*, *Phys. Rev.* **D 65** (2002) 074037 [hep-ph/0110325].

[8] J. Kwiecinski and A.M. Stasto, *Geometric scaling and QCD evolution*, *Phys. Rev.* **D 66** (2002) 014013 [hep-ph/0203030].

[9] S. Munier and R. Peschanski, *Geometric scaling as traveling waves*, *Phys. Rev. Lett.* **91** (2003) 232001 [hep-ph/0309177].

[10] S. Munier and R. Peschanski, *Universality and tree structure of high energy QCD*, *Phys. Rev.* **D 70** (2004) 077503 [hep-ph/0401215].

[11] E. Iancu and D.N. Triantafyllopoulos, *A Langevin equation for high energy evolution with pomeron loops*, *Nucl. Phys.* **A 756** (2005) 419 [hep-ph/0411405].

[12] E. Iancu, A.H. Mueller and S. Munier, *Universal behavior of QCD amplitudes at high energy from general tools of statistical physics*, *Phys. Lett.* **B 606** (2005) 342 [hep-ph/0410018].

[13] E. Avsar, G. Gustafson and L. Lonnblad, *Energy conservation and saturation in small-X evolution*, *JHEP* **07** (2005) 062 [hep-ph/0503181].

[14] E. Avsar, G. Gustafson and L. Lonnblad, *Small-X dipole evolution beyond the large-N_c limit*, *JHEP* **01** (2007) 012 [hep-ph/0610157].

[15] A.H. Mueller, *Soft gluons in the infinite momentum wave function and the BFKL pomeron*, *Nucl. Phys.* **B 415** (1994) 373.

[16] A.H. Mueller and B. Patel, *Single and double BFKL pomeron exchange and a dipole picture of high-energy hard processes*, *Nucl. Phys.* **B 425** (1994) 471 [hep-ph/9403256].

[17] A.H. Mueller, *Unitarity and the BFKL pomeron*, *Nucl. Phys.* **B 437** (1995) 107 [hep-ph/9408245].

[18] S. Catani, F. Fiorani and G. Marchesini, *QCD coherence in initial state radiation*, *Phys. Lett.* **B 234** (1990) 339.

[19] M. Ciafaloni, *Coherence effects in initial jets at small Q^2/s*, *Nucl. Phys.* **B 296** (1988) 49.

[20] B. Andersson, G. Gustafson and J. Samuelsson, *The linked dipole chain model for dis*, *Nucl. Phys.* **B 467** (1996) 443.

[21] G.P. Salam, *Soft emissions and the equivalence of BFKL and CCFM final states*, *JHEP* **03** (1999) 009 [hep-ph/9902324].

[22] G.P. Salam, *Oedipus: onium evolution, dipole interaction and perturbative unitarisation simulation*, *Comput. Phys. Commun.* **105** (1997) 62 [hep-ph/9601220].

JHEP04(2007)067

[23] G.P. Salam, *Studies of unitarity at small-x using the dipole formulation*, *Nucl. Phys.* **B 461** (1996) 512 [hep-ph/9509353].

[24] G.P. Salam, *An introduction to leading and next-to-leading BFKL*, *Acta Phys. Polon.* **B30** (1999) 3679 [hep-ph/9910492].

[25] L.H. Orr and W.J. Stirling, *Dijet production at hadron hadron colliders in the BFKL approach*, *Phys. Rev.* **D 56** (1997) 5875 [hep-ph/9706529].

[26] J.R. Andersen and W.J. Stirling, *Energy consumption and jet multiplicity from the leading log BFKL evolution*, *JHEP* **02** (2003) 018 [hep-ph/0301081].

[27] H1 collaboration, C. Adloff et al., *Deep-inelastic inclusive e P scattering at low X and a determination of α_s*, *Eur. Phys. J.* **C 21** (2001) 33 [hep-ex/0012053].

[28] ZEUS collaboration, J. Breitweg et al., *Measurement of the proton structure function F2 at very low Q^2 at HERA*, *Phys. Lett.* **B 487** (2000) 53 [hep-ex/0005018].

[29] G. Gustafson and G. Miu, *A simple model for the BFKL-DGLAP transition in deep inelastic scattering*, *Eur. Phys. J.* **C 23** (2002) 267 [hep-ph/0110143].

[30] F. Gelis, R. Peschanski, G. Soyez and L. Schoeffel, *Systematics of geometric scaling*, *Phys. Lett.* **B 647** (2007) 376 [hep-ph/0610435].

[31] G. Gustafson, *An intuitive semiclassical picture of proton structure at small X*, *Acta Phys. Polon.* **B34** (2003) 2963 [hep-ph/0306108].

[32] S. Munier, *Geometric scaling in a symmetric saturation model*, *Phys. Rev.* **D 66** (2002) 114012 [hep-ph/0205319].

[33] V.P. Goncalves and M.V.T. Machado, *Saturation physics in ultra high energy cosmic rays: heavy quark production*, hep-ph/0607125.

[34] ZEUS collaboration, S. Chekanov et al., *Measurement of $d^{*\pm}$ production in deep inelastic $e^{\pm}$ P scattering at HERA*, *Phys. Rev.* **D 69** (2004) 012004 [hep-ex/0308068].

[35] H.G. Dosch, T. Gousset and H.J. Pirner, *Nonperturbative γ^* p interaction in the diffractive regime*, *Phys. Rev.* **D 57** (1998) 1666 [hep-ph/9707264].

[36] S. Munier, *Cross-fertilization of QCD and statistical physics: high energy scattering, reaction-diffusion, selective evolution, spin glasses and their connections*, *Acta Phys. Polon.* **B37** (2006) 3451 [hep-ph/0609161].

JHEP04(2007)067